Computational laboratories, test case 1

Laminar oil transport in a pipeline

Francesco Derme, Pietro Di Giustino, Pietro Fumagalli

1 Introduction

We simulate the transport of a heavy crude oil in a pipe, precisely we consider: density $\rho = 910\frac{kg}{m^3}$, kinematic viscosity $\nu = 3.5 \cdot 10^{-4}\frac{m^2}{s}$, pipe diameter $d = 150mm$ and bulk velocity $W_b = 0.45\frac{m}{s}$. The steady-state formulation of the Navier-Stokes are solved with inlet, outlet, wall and axis boundary conditions. Note that the length of the pipe is not specified, indeed given this setting it's reasonable to expect the flow to become fully developed at a certain distance from the inlet. The search for a length L that doesn't induce excessive computational complexity while being big enough to let the transitory stage of the flow come to an end and to appreciate the effects of fully developed flow is part of the problem itself. The fully developed part of the flow, i.e. the part of the flow that is located downstream of the entry length L_e, will be of interest for our analysis.

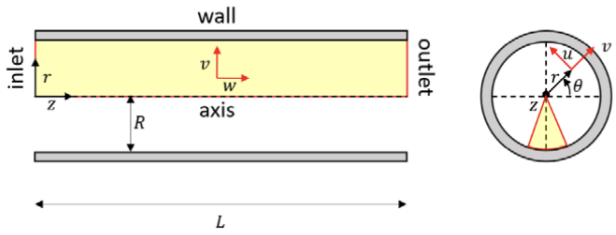

2 Analysis

1. In order to verify that the conditions induce a laminar flow, the Reynolds bulk number Re_b is calculated. The velocity to be used in this computation is the bulk velocity (it would make no sense to use the axial velocity which depends on the specific coordinates, the bulk velocity is instead constant along the length of the pipe as a result of mass conservation). As proven below, the flow is laminar.

$$Re_b = \frac{W_b \cdot D}{\nu} = \frac{0.45 \cdot 0.15}{3.5 \cdot 10^{-4}} \simeq 192 < 2000 \tag{1}$$

2. The pipe length is set to $L = 2.5m$. The goal is to set L in such a way that the fully developed flow conditions can be attained from the uniform velocity profile imposed at the inlet. Recall that the flow is fully developed when the axial derivative of all the variables, except for the pressure, is null. To validate our choice we initially use a qualitative criterion: looking at the axial velocity profile it's clear that it doesn't change much along z after 2 meters or so, as shown in the image below.

We define a custom quantitative criterion in order to strengthen the claim that the flow is fully developed after about 2 meters. The idea is to compute the incremental ratio of the centerline velocity (the centerline is where maximum speed is reached). We take two adjacent cells along z, subtract the velocities stored in those cells and then normalize this difference by the length of a single cell (all the grids used are uniform along the z-axis, so the length of every cell is the same). Finally, we define L_e as the distance from the inlet where the incremental ratio drops below 0.01. Of course the choice of 0.01 is arbitrary but, as described below, this leads to a criterion that is more restrictive than the ones found in the literature. By this definition $L_e = 1.975$.

The image below shows two simulations run with the same settings except for the pipe's length: in the first case $L = 2.5m$ and in the second $L = 5m$. The green horizontal line is the velocity that we expect to see in the centerline when the flow is fully developed. It's clear that that target velocity is reached in both simulations, so we decide to set the length of the pipe to $L = 2.5m$ for all the following simulations as we are confident this allows experiencing the fully developed state while not increasing the computational cost too much.

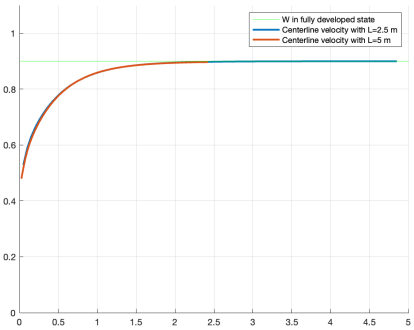

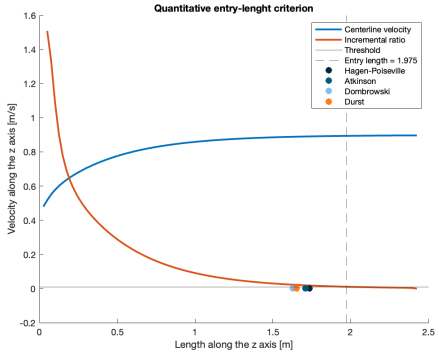

We select some metrics for L_e from the literature and compare them to our custom criterion:

- Hagen-Poiseville: $L \simeq 0.06 \cdot Re_b \cdot d = 1.7357m$
- Atkinson: $L \simeq (0.59 + 0.056 \cdot Re_b) \cdot d = 1.7085m$
- Dombrowski: $L \simeq (0.379 \cdot e^{-0.148 \cdot Re_b} + 0.055 \cdot Re_b + 0.26) \cdot d = 1.6301m$
- Durst: $L \simeq (0.619^{1.6} + (0.0567 \cdot Re_b)^{1.6})^{1/1.6} \cdot d = 1.6506m$

As shown in the image above, all these criterion are less restrictive than ours.

3. The solution is physically, qualitatively sound. The color plots don't exhibit any strange pattern, instead the variables behave exactly as expected with the θ and r components of the velocity being null and the axial velocity being maximal in the center of the pipe. The pressure, as one would expect, decreases linearly since this is a pressure-driven flow. The image below shows the pressure decreasing, while velocity profile can be appreciated in the previous figures.

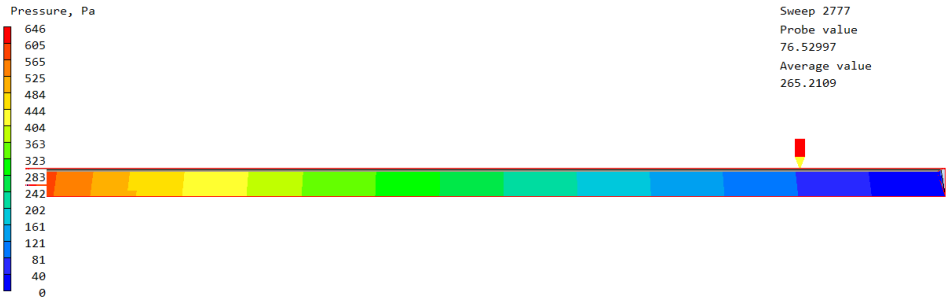

4. We verified the numerical convergence of the produced simulation in terms of both the numerical convergence of the solution algorithm and grid independence. As far as the convergence with respect to the algorithm, plotted below are the normalized whole-field residuals and probe values: the first tend to 0, or rather they stabilize below the threshold of 10^{-3}, the second converge to a fixed value, respecting our convergence criteria long before the maximum number of iterations was reached.

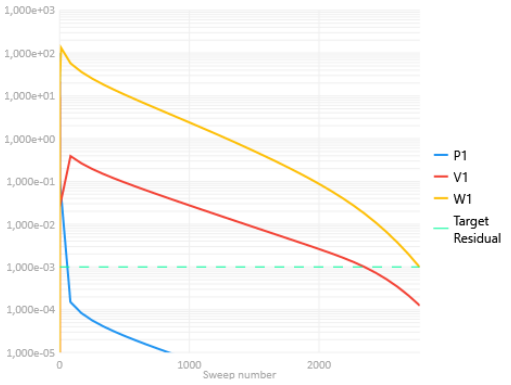

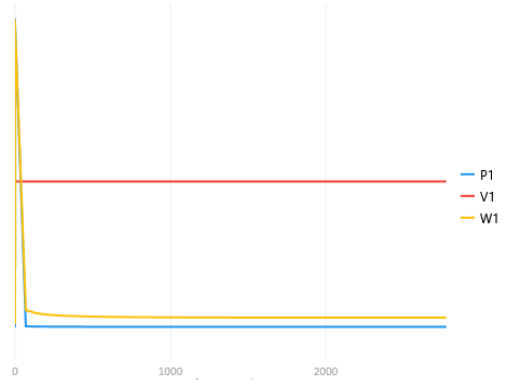

Variable	Value	Low	High	ValueChange
P1	3,078e-08	3,078e-08	8,217e+22	-3,179e-05
V1	1,245e-04	1,245e-04	3,334e+26	-1,287e-01
W1	9,866e-04	9,866e-04	3,589e+27	-1,028e+00

Sweep:2777 | Step:1 (100,0%)

Time elapsed: 0h 0m, remaining: 0h 1m
Current directory: C:\phoenics\d_priv1

Variable	Value	Low	High	ValueChange
P1	7,140e+01	7,140e+01	7,140e+07	-7,133e+04
V1	0,000e+00	0,000e+00	0,000e+00	0,000e+00
W1	1,805e-02	1,805e-02	1,805e+04	-1,803e+01

Sweep:2777 | Step:1 (100,0%)

Time elapsed: 0h 0m, remaining: 0h 1m
Current directory: C:\phoenics\d_priv1

The target parameters of the grid independence study are W, $\frac{dW}{dy}$ and P, all of which have been proven grid-independent. We investigated increasing mesh refinement levels along both the z and r directions separately. In particular, the tested meshes are shown in the table below.

Mesh name	# cells along x	# cells along y	# cells along z	Power law
Base case	1	26	100	No
z ref 1	1	26	250	No
z ref 2	1	26	500	No
y ref 1	1	50	100	No
y ref 2	1	100	100	No
y pl ref 1	1	25	100	Yes
y pl ref 2	1	30	100	Yes
y pl ref 3	1	35	100	Yes
y pl ref 4	1	40	100	Yes
y pl ref 5	1	45	100	Yes
y pl ref 6	1	50	100	Yes
y pl ref 7	1	55	100	Yes
y pl ref 8	1	60	100	Yes
y pl ref 9	1	65	100	Yes
y pl ref 10	1	85	100	Yes

The power law has always been applied with a power of -1.5.

All the meshes are based on cylindrical-polar coordinates. These mesh patterns were of interest to our analysis because we wanted to test the hypothesis that increasing the mesh refinement level along the axial coordinate wouldn't have caused a significant shift in the simulation results, indeed this was the case. Increasing the refinement level along the r direction was more problematic because it would lead the simulation closer and closer to the wall and, particularly when the power-law was enabled, it could stretch out the cells too much and create numerical instabilities. Ultimately the chosen grid was **y ref 2** since it was relatively computationally cheap while definitively being fine enough to prove the test variables grid independent, this can be seen in full in the following graphs.

In addition to visual inspection, we formulate a quantitative criterion to test grid independence. After interpolating the values of W, $\frac{dW}{dy}$ and P on their respective storage points on the coarser meshes, we calculated a **pseudo-L_1 norm** of the difference of the test variables. This was done by calculating the sum of the absolute values of the point-wise differences of the variables being compared and then normalizing this sum by diving it by the number of cells in the coarser mesh. Note that the interpolation was performed with respect to z in the computation of L_1 norms for P and W, with respect to y in the computation of the L_1 norm for $\frac{dW}{dy}$. Once again, these results, even if they follow from a somewhat arbitrary definition of a norm, increase the solidity of our approach and prove once more that our findings are grid-independent.

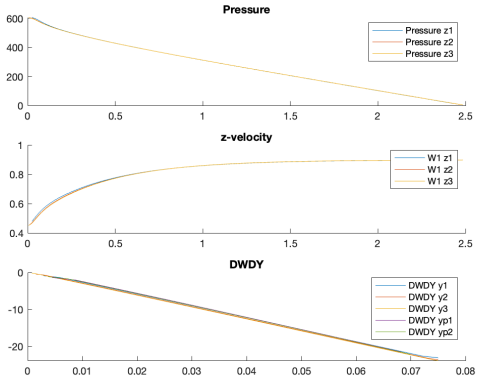

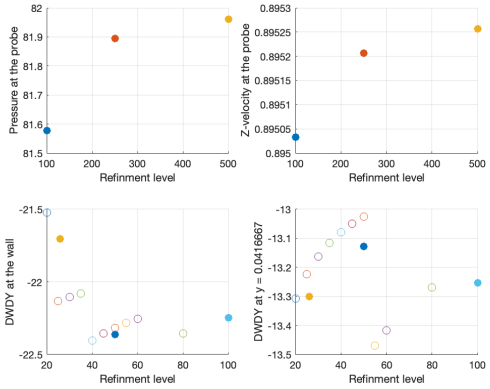

Meshes	variable	L_1 norms
z ref 1 vs **z ref 2**	P	0.53976
z ref 2 vs **z ref 3**	P	0.11452
z ref 1 vs **z ref 3**	P	0.65352
z ref 1 vs **z ref 2**	W	0.0018505
z ref 2 vs **z ref 3**	W	0.00075712
z ref 1 vs **z ref 3**	W	0.0026041

Meshes	variable	L_1 norms
y ref 1 vs **y ref 2**	dW/dy	0.22573
y ref 2 vs **y ref 3**	dW/dy	0.11839
y ref 1 vs **y ref 3**	dW/dy	0.33645
y pl ref 1 vs **y pl ref 2**	dW/dy	0.095547
y ref 3 vs **y pl ref 2**	dW/dy	0.3148

5. The fully developed laminar flow in a pipe admits an analytical solution, the cylindrical Poiseuille flow. We perform **benchmarking** by manipulating the above equations and writing $\frac{dp_e}{dz}$ as a function of W_b which is given.

$$w(r,\theta,z) = -\frac{1}{4\mu}\frac{dp_e}{dz}(R^2 - r^2) \quad u(r,\theta,z) = 0 \quad v(r,\theta,z) = 0$$

$$\frac{dp_e}{dz} = const < 0$$

$$\tau_{rz}(r,\theta,z) = -2\mu\frac{1}{2}(\frac{\partial v}{\partial z} + \frac{\partial w}{\partial r}) = -\mu\frac{\partial w}{\partial r} = \frac{dp_e}{dz}\frac{r}{2}$$

$$Q = \int_0^R w(r)2\pi R\,dr = -\frac{1}{4\mu}\frac{dp_e}{dz}\int_0^R (R^2 - r^2)2\pi R\,dr = -\frac{2\pi}{4\mu}\frac{dp_e}{dz}\frac{R^4}{4} \implies$$

$$\implies W_b = \frac{Q}{\pi R^2} \quad W_b = -\frac{1}{2}\frac{dp_e}{dz}\frac{R^2}{4} \implies \frac{dp_e}{dz} = -\frac{8\mu}{R^2}W_b = -\frac{8\nu\rho}{R^2}W_b = -203.84$$

$$\implies w(r,\theta,z) = w(r) = 160 \cdot (R^2 - r^2) \quad \tau_{rz}(r,\theta,z) = \tau_{rz}(r) = 101.92 \cdot r$$

Given the theoretical results of the Poiseuille flow, the goal is now to compare them to the ones obtained through the simulation. Concerning the pressure gradient, we define the predicted $\frac{dp_e}{dz}$ by taking the difference of the pressure in two points $0.5m$ apart (in the fully developed region). We expect this difference to be close to $\frac{-203.84}{2} = -101.92$ and we find a difference of less than 1%.

For a qualitative check of the axial velocity profile and the shear stress we plot these variables, both the theoretical and the predicted ones.

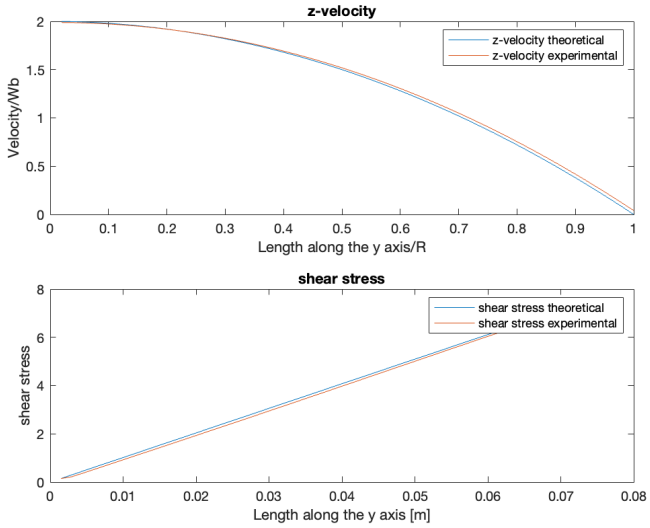

We also compute the L1 norm of the difference between the theoretical and the predicted variables, obtaining excellent results (L1-norm of Wexact versus Wpredicted = 0.0089317, L1-norm of Wexact versus Wpredicted = 0.090716).

6. To obtain the trend of the friction factor f versus the bulk Reynolds number Re_b, we work on the definition of the friction coefficient and of the hydraulic gradient J:

$$C_f = \frac{\tau_w}{\frac{1}{2}\rho W_b^2} = \frac{-\frac{dp_e}{dz}\frac{R}{2}}{\frac{1}{2}\rho W_b(-\frac{1}{8}\mu\frac{dp_e}{dz}R^2)} = \frac{1}{\frac{\rho W b R}{8\mu}} = \frac{16}{\frac{\rho W b(2R)}{\mu}} = \frac{16}{Re_b}$$

$$J = -\frac{1}{\gamma}\frac{dp_e}{dz} = f\frac{W_b^2}{2g(2R)} \implies f = -\frac{\frac{1}{\gamma}\frac{dp_e}{dz}}{\frac{\gamma W_b^2}{2g(2R)}} = \frac{\tau_w}{\frac{\rho w_b^2}{8}} = \frac{4\tau_w}{\frac{1}{2}\rho W_b^2}$$

$$f = 4C_f \implies f = \frac{64}{Re_b}$$

We obtain the theoretical trend by substituting the values for W_b, d and ρ in the formula for Re_b. Next, we compare the analytical solution with the value of f computed through CFD, this can be obtained by plugging τ_w into the equation above. The percentage difference we find between theoretical and computational results is less than 1%. We modify W_b and d, always ensuring that Re_b remains below the threshold value of 2000, and repeat the calculations finding similar results. This close match strengthens our findings and the validity of out CFD simulations.

W_b	d	threshold
0.45	**0.15**	1%
0.55	**0.25**	1%
0.7	**0.4**	5%
1	**0.6**	1%